Mott insulator to correlated metal: Optical study of $La_{1-x}TiO_3$

D. A. Crandles
Memorial University, Grenfell College, Corner Brook, Newfoundland, Canada A2H 6P9

T. Timusk
Department of Physics and Astronomy and Institute for Materials Research, McMaster University, Hamilton, Ontario, Canada L8S 4M1

J. D. Garrett
Institute for Materials Research, McMaster University, Hamilton, Ontario, Canada L8S 4M1

J. E. Greedan
Department of Chemistry and Institute for Materials Research, McMaster University, Hamilton, Ontario, Canada L8S 4M1
(Received 18 January 1994)

The room-temperature reflectance of a well-characterized series of samples (x-ray, neutron activation and thermigravimetric analyses, resistivity, magnetization) in the $La_{1-x}TiO_3$ system has been measured between 50 and 40 000 cm^{-1} on samples ranging from the antiferromagnetic insulating ($LaTiO_3$) to the metallic ($La_{0.88}TiO_3$) part of the phase diagram. The electronic portion of the low-frequency optical conductivity *increases* with frequency at the lowest frequencies, similar to several barely metallic systems. This non-Drude behavior can be modeled as the sum of the two low-frequency oscillators, a Drude contribution that increases systematically with doping and a broad midinfrared continuum. The midinfrared band, which may be associated with transitions across the Hubbard gap, persists in highly doped samples in agreement with theoretical predictions. If one assumes a single low-frequency component with frequency-dependent scattering rate, one finds a negative mass enhancement below 150 cm^{-1} in metallic samples close to the metal-insulator phase boundary.

I. INTRODUCTION

There has been tremendous interest in d^1 systems recently as part of the study of electron correlation in narrow band systems. In particular, stoichiometric $LaTiO_3$ is a d^1 compound just on the insulating side of the Mott-Hubbard transition ($U/W \sim 1$).[1-4] $La_xSr_{1-x}TiO_3$ is an ideal system for determining the influence of band filling on electronic properties since the end members $SrTiO_3$ and $LaTiO_3$ have d^0 and d^1 configurations, respectively. For small x, the system behaves like a Fermi liquid while at $x_c \sim 0.95$ a metal-insulator transition takes place. Perhaps the most interesting observations on $La_xSr_{1-x}TiO_3$ have been the systematic increases in the Pauli magnetic susceptibility and the T-linear coefficient of the specific heat near the metal-insulator phase boundary, which indicate a filling-dependent critical enhancement of the effective mass.[5,6] The system has also been studied using x-ray diffraction, resistivity, photoemission, and reflectance.[7-10]

The first goal of this paper is to discuss a different way to control the metal-insulator transition in $LaTiO_3$. For La-deficient samples have been prepared ranging from the antiferromagnetic insulating ($LaTiO_3$) to the metallic part of the phase diagram ($La_{0.88}TiO_3$). Chemical analysis indicates that oxidized samples exhibit stoichiometry $La_{1-x}TiO_3$ rather than stoichiometry $LaTiO_{3+x}$ as had been suggested by Lichtenberg *et al.*[1]

The second purpose of this paper is to present data regarding the evolution of the optical conductivity across the Mott-insulator–correlated-metal phase boundary. It is now common to use the Zaanen, Sawatsky, and Allen (ZSA) scheme to classify correlated insulators.[11] In this scheme a material is a Mott-Hubbard insulator if the smallest energy gap is that required for the charge fluctuation $d^n + d^n \rightarrow d^{n+1} + d^{n-1}$ or a charge-transfer insulator if the smallest energy gap is the anion-cation charge-transfer energy. High-T_c superconductivity occurs when certain antiferromagnetic charge-transfer insulators are doped. Understandably, there has been considerable interest in how the physical properties of highly correlated insulators evolve with doping. The room-temperature optical conductivity has been studied as a function of doping in various charge-transfer insulators[12-15] and recently in the Mott-Hubbard systems $Y_{1-x}Ca_xTiO_3$ (Ref. 16) and $Y_{1-x}Ca_xVO_3$.[17] Doping introduces the so-called midinfrared band in each and every one of these systems. One observes that in the $La_{1-x}TiO_3$ system, the electronic portion of the low-frequency optical conductivity is not Drude-like: it *increases* with frequency at the lowest frequencies measured. The electronic portion of the low-frequency dielectric function can be modeled as the sum of a Drude component and a midinfrared band. The strength of the Drude component increases systematically with increased doping while the broad midinfrared continuum, which may be associated with transitions across the Hubbard

gap, persists in highly doped samples. Alternatively, one can model the low-frequency optical conductivity using a single component with a frequency-dependent mass enhancement and scattering rate. Close to the Mott-Hubbard metal-insulator transition, correlation-induced mass enhancements are expected to occur. However, one finds a negative mass enhancement in a metallic sample below 150 cm^{-1}. This result is contrasted with optical data concerning electron mass enhancements below the coherence temperature in heavy fermion materials.

II. EXPERIMENT

A. Sample preparation and characterization

Four twinned[18] crystals labeled *A*, *B*, *C*, and *D* were studied. Figure 1 shows the temperature dependence of the resistivity of the four samples. Sample *A* exhibits an insulatorlike negative temperature coefficient of resistivity for all temperatures between 4 and 300 K. Sample *B* exhibits a change from insulating to metallic behavior near 175 K, while samples *C* and *D* show metallic resistivity behavior between 4 and 300 K. No attempt was made to look for a superconducting transition below 4 K. The temperature dependence of the magnetization for these crystals appears in Fig. 2. In agreement with the data of Lichtenberg *et al.*, the Neél temperature systematically decreases as the room-temperature resistivity decreases.[1] $LaTiO_3$ exhibits antiferromagnetic ordering so the small moments seen in Fig. 2 are due to canting of adjacent spins.[19]

Crystals *A*, *B*, and *C* were prepared by a technique described previously.[18] They were not intentionally doped yet these samples exhibit strikingly different physical properties. Chemical analysis reveals that the variations are due to differing amounts of La vacancies. While the target stoichiometry of sample *D* was $LaTiO_{3.10}$, analysis showed that the boule was inhomogeneous and the stoichiometry of the piece used for the optical measurement was $La_{0.88}TiO_3$. Starting material for sample *D* was mixed according to the following reaction:

$$La_2O_3+(1-2x)Ti_2O_3+4xTiO_2 \rightarrow 2LaTiO_{3+x} .$$

The boule from which sample *D* was cut was produced in two steps. First, the precursor material was arc melted under argon. Second, a button of polycrystalline material was melted in the water-cooled hearth of a modified Reed-type Tri-arc furnace and using a tunsten rod as a seed, the crystal was pulled from the melt. The growth rate was 25 mm/h while the water-cooled seed rod and hearth were rotated at 60 and 120 rpm, respectively, in opposite directions.

Sample purity and lattice constants were determined by x-ray diffraction using a Guinier camera. The cation ratios were checked using neutron-activation analysis and the weight gains upon heating the samples to 1000 °C in air were measured, and all these results appear in Table I.

In summary, one can make several observations on the $La_{1-x}TiO_3$ system close to stoichiometry $LaTiO_3$. The system crystallizes in the $GdFeO_3$ structure, and as the

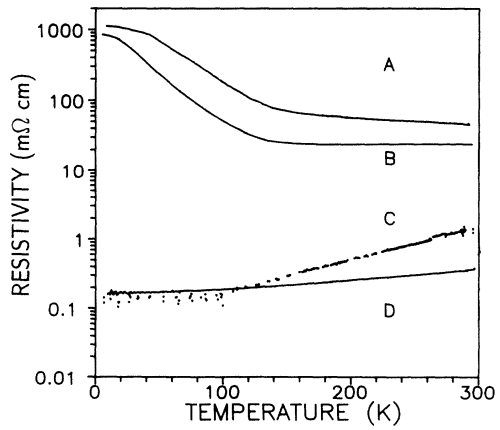

FIG. 1. Resistivity of the four $La_{1-x}TiO_3$ samples used in the reflectance measurements.

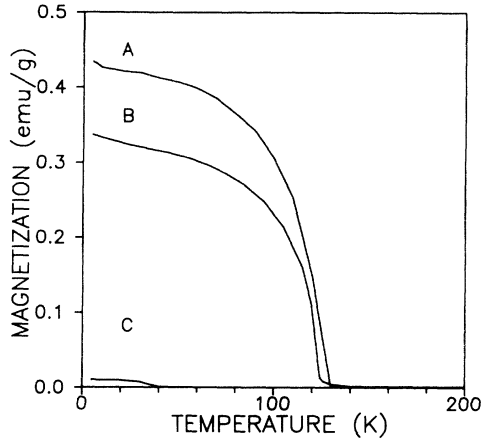

FIG. 2. Magnetization as a function of temperature for samples *A*, *B*, and *C*. These samples were cooled in zero field. The moment was established by ramping the field to 15 kG. The field was then reduced to zero and the sample warmed in zero field. Sample *D* had a smaller moment than sample *C* with onset at lower temperature.

TABLE I. Chemical analysis of samples *A*, *B*, *C*, and *D*. The La:Ti ratio was determined by neutron-activation analysis. The thermogravimetric analysis weight gains were determined while heating to 1000°C in air. The difference in uncertainty are due to the different amounts of material available for oxidation. The unit-cell volumes were measured using a Guinier camera.

Sample	La:Ti (±0.045)	% weight gain	Cell volume ($Å^3$)
A	0.97	3.4±0.5	249.93(3)
B	0.96	3.18±0.15	249.14(3)
C	0.93	2.7±0.5	247.76(7)
D	0.88	2.3±0.1	244.69(6)

La content decreases, the unit cell shrinks, the thermogravimetric weight gain decreases (the samples are more oxidized), the resistivity decreases (the samples become more metallic), and the Neél temperature decreases. This is similar to the work of Lichtenberg *et al.*,[1] who maintain that these systematic changes are due to excess oxygen ($LaTiO_{3+x}$). In contrast, our neutron-activation results indicate La vacancies rather than excess oxygen ($La_{1-x}TiO_3$). This is especially clear for sample *D* where we intended to create a sample containing excess oxygen, but ended with a sample containing La vacancies. The cation vacancy model makes more sense on structural grounds. It is hard to see where the large O^{2-} ion could be forced into the close-packed perovskite lattice and difficult to understand how large interstitial ions could cause the unit cell to shrink. Finally, one knows that the perovskite structure is maintained down to stoichiometry $La_{2/3}TiO_3$[20] and solid solutions are conceivable. Structural investigations are now in progress, which should confirm the cation vacancy model for oxidized $LaTiO_3$.

B. Optical measurements

The samples were mechanically polished for the optical measurements. The absolute reflectance of the samples was determined via an *in situ* evaporation technique[21] using a Michelson interferometer between 70 and 5500 cm^{-1} and grating spectroscopy between 4000 and 40 000 cm^{1}. The uncertainty in the measurements is about 1% between 70 and 700 cm^{-1}, and about 2% for higher frequencies. Kramers-Kronig analysis was performed in order to see the doping-induced changes in the optical conductivity. Constant low-frequency reflectance was assumed for samples *A* and *B*, while the reflectance of samples *C* and *D* was extended to low frequencies using a Drude extrapolation consistent with the measured dc resistivity. A variety of high-frequency extrapolations were used based on the high-frequency reflectance of nominally stoichiometric $LaTiO_3$ measured by Fujishima *et al.*[10] or Cardona's measurements of the reflectance of $SrTiO_3$.[22] The optical-conductivity spectra below 10 000 cm^{-1} are insensitive to the high-frequency extrapolation.

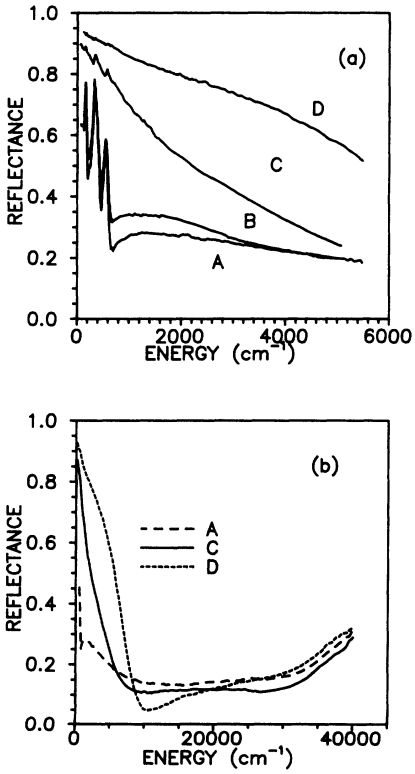

FIG. 3. (a) 300-K reflectance of samples *A*, *B*, *C*, and *D* from the far infrared to midinfrared. (b) 300-K reflectance of samples *A*, *C*, and *D* in the near infrared to visible spectral region. Samples *C* and *D* show metallic behavior, whereas samples *A* and *B* have the optical properties of an insulator.

III. REFLECTANCE AND OPTICAL CONDUCTIVITY

Figures 3(a) and 3(b) present the room-temperature reflectance of samples *A*, *B*, *C*, and *D*. Besides the phonon peaks near 170, 340, and 560 cm^{-1}, the reflectance data indicate the presence of three different electronic-absorption processes: a midinfrared process associated with the nonzero reflectance above the highest frequency optical phonon in the insulating samples, a visible absorption that causes the increase in reflectance above 30 000 cm^{-1} in all the samples, and low-frequency free-carrier absorption in metallic samples *C* and *D*. The visible transition is due to O(2*p*)-Ti(3*d*) charge transfer. The midinfrared absorption, which exists in all $RTiO_3$ perovskites (R=La, Ce, Pr, Nd, Sm, Gd), may correspond to excitations from the lower to the upper Hubbard subbands.[2] Because the smallest optical gap is *U*, stoichiometric $LaTiO_3$ is a Mott-Hubbard insulator in the ZSA phase diagram. The free-carrier component grows with the number of La vacancies and causes the systematic increase in low-frequency reflectance and the development of a plasma edge that moves to higher frequencies as shown in Fig. 3(b).

In Fig. 4, the real part of the optical conductivity is

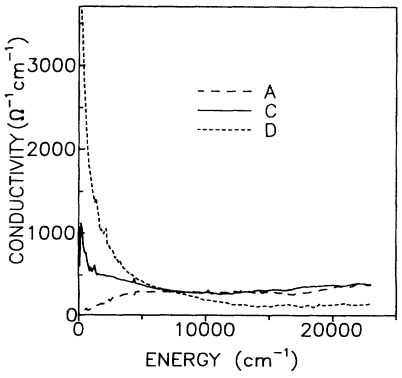

FIG. 4. Room-temperature optical conductivity vs frequency for samples *A*, *C*, and *D*. All samples show a midinfrared band. In addition samples *C* and *D* have a free-carrier low-frequency band.

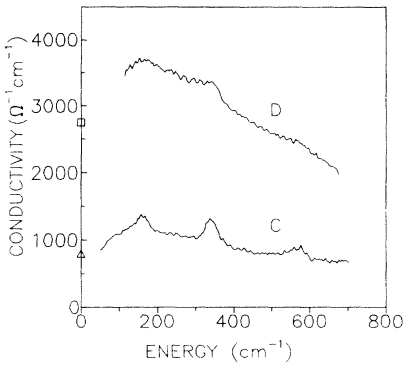

FIG. 5. Low-frequency optical conductivity for metallic samples C and D. The triangle and square on the conductivity axis are the dc conductivity of samples C and D, respectively. The positive slope of the conductivity behavior at low frequency suggests localization of the carriers.

shown for samples A, C, and D. Note the gaplike feature below the midinfrared absorption in the spectrum of insulating sample A and increased spectral weight at low frequencies for La-deficient samples C and D. The transfer of spectral weight from above 10 000 cm^{-1} to low frequencies in sample D is an indication that $LaTiO_3$ is a strongly correlated system. A density of states that is highly sensitive to doping is one of the characteristics which distinguishes a correlated insulator from a Bloch-Wilson (filled band) insulator.[23] With the layered cuprates, one can clearly see a transfer of spectral weight from high energies (the charge-transfer gap) to low energies. It is curious that there does not appear to be any spectral-weight transfer in sample C. It may be that it is obscured by the increased uncertainty in the Kramers-Kronig derived spectral functions above 10 000 cm^{-1}.

Figure 5 shows the non-Drude behavior of the low-frequency optical conductivity of metallic samples C and D. At the lowest measured frequencies, the optical conductivity increases with increasing frequency, but appears consistent with the dc conductivity, which is also shown in the diagram. It is interesting to note that similar behavior has been observed in the metallic phase of V_2O_3, the classic Mott-Hubbard material.[24] It is also reminiscent of other marginally metallic systems such as the quasicrystals[25] and doped-compensated semiconductors.[26]

IV. ANALYSIS AND DISCUSSION

An increase in optical conductivity with frequency can be described by two low-frequency components. We use a dielectric function consisting of a sum of independent Lorentzian oscillators. We include Lorentzians for the phonons, the high-frequency charge-transfer process, and an overdamped Lorentzian for the midinfrared absorption. Finally, a Drude oscillator is included to allow for absorption by the itinerant carriers. To begin, the parameters for the dielectric function of insulating sample A were obtained by fitting the reflectance and conductivity. For the fits of the more metallic samples, ϵ_∞ and the charge-transfer oscillator constants were held fixed while the rest of the parameters were allowed to vary. The fitting parameters appear in Table II, while the reflectance fits can be compared with the experimental data for samples A and D in Fig. 6.

This model is consistent with the picture that stoichiometric $LaTiO_3$ is a Mott-Hubbard insulator in the ZSA phase diagram.[2,27] In the insulating samples, the midinfrared component would correspond to excitations from the lower to the upper Hubbard band, that is excitations which place two electrons on one Ti site. The high-frequency Lorentzian is associated with O($2p$)-Ti($3d$) charge transfer. In Fig. 7, one can compare the measured optical conductivity to the midinfrared and Drude components. In our model, the midinfrared component narrows and shifts to lower frequencies with increased doping, but exists even in the highly doped metallic samples C and D. This is consistent with reflectance studies of the hole-doped Mott-Hubbard insulators $Y_{1-x}Ca_xTiO_3$ and $Y_{1-x}Ca_xVO_3$,[16,17] where one can clearly see persistence of a pseudogap in the optical conductivity in metallic samples. The doping dependence of the optical conductivity in the titanite systems $La_{1-x}TiO_3$ and $Y_{1-x}Ca_xTiO_3$ is different than in the cuprates, where the optical feature associated with the charge-transfer gap persists in doped samples alongside a midinfrared band. With the titanites, the fundamental absorption edge in the insulating samples appears to evolve smoothly into the midinfrared band in the metallic samples. A recent photoemission study of d^1 perovskites also revealed the persistence of Hubband bands on the metallic side of the Mott-Hubbard transition in metallic samples of VO_2, $SrVO_3$ and $LaTiO_3$.[28] There is theoreti-

TABLE II. Parameters for the sum model fits to the reflectance and optical conductivity for samples A, B, C, and D. Lorentzians 1–3 represent phonons, while Lorentzians D and M represent the Drude and midinfrared oscillators discussed in the text. $\epsilon_\infty = 3.92$, while the center frequency, width, and plasma frequency of the visible oscillator are 39 600, 4900, and 37 000 cm^{-1}, respectively. In the table, all frequencies and dampings are in cm^{-1}.

		A			B	
i	ω_{0i}	Γ_i	ω_{pi}	ω_{0i}	Γ_i	ω_{pi}
1	170	20	600	169	22	640
2	340	56	1100	338	64	1260
3	545	52	720	548	60	830
D	0	540	1100	0	280	1080
M	6600	22 700	19 400	4130	13 600	15 700
		C			D	
i	ω_{0i}	Γ_i	ω_{pi}	ω_{0i}	Γ_i	ω_{pi}
1	160	35	820	172	49	920
2	340	30	930	340	139	1650
3	571	32	605	565	81	900
D	0	360	4280	0	430	9000
M	890	9100	16 300	655	3400	15 500

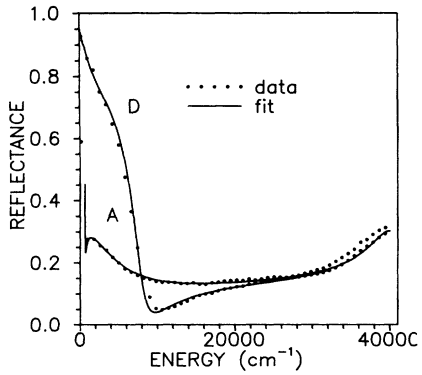

FIG. 6. Reflectance of the most metallic and most insulating samples (*D* and *A*, respectively) compared with the sum model fits.

cal evidence for the persistence of spectral weight associated with placing two electrons on one site in highly doped samples. The optical conductivity has been calculated numerically for the Hubbard model on a 3×3 lattice as a function of doping.[29] These calculations have shown that the feature in the optical-conductivity spectrum associated with the upper Hubbard band persists even when only half the sites are filled. However, the peak of the band does not move to lower frequencies in these models.

It is interesting that Fujimori find a feature near 1.5 eV from the Fermi level in the photoemission spectra of $La_xSr_{1-x}TiO_3$ down to $x\sim0.1$.[9,28] They note that the usual Hubbard model with on-site repulsion cannot explain the feature for such a low site occupation. It would be interesting to explore the doping dependence of the optical conductivity in an extended Hubbard model, which includes nearest-neighbor or even second-nearest-neighbor repulsion. Perhaps the feature associated with the upper Hubbard band would persist to even lower site occupations than where half the sites are occupied. This leads one to reconsider the midinfrared band in *n*-type $SrTiO_3$ where, almost 30 years ago, a midinfrared absorption was reported,[30] the origin of which remains controversial. Various explanations have been offered for this absorption, including small polaron absorption[31] and, most recently, intraband scattering.[32] It is possible that the midinfrared band in both *n*-type $SrTiO_3$ and in $LaTiO_3$ have the same origin, associated with placing two electrons on one site.

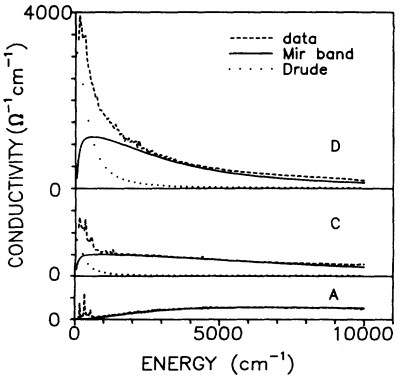

FIG. 7. Comparison of the measured $\sigma(\omega)$ of the $La_{1-x}TiO_3$ system with the Drude and midinfrared components of the sum model fits.

Alternatively, one can consider the non-Drude optical conductivity of $La_{1-x}TiO_3$ to arise from a single low-frequency contribution to the dielectric function with frequency-dependent scattering rate and mass enhancement. This is suggested by optical observations of low-temperature mass enhancements in heavy-fermion materials.[33,34] In the generalized Drude formalism,[35] the usual expression for the conductivity, which is obtained from a dielectric function consisting of a Lorentzian of width Γ and strength ω_p^2 placed at the origin, becomes

$$\sigma(\omega)=\frac{1}{4\pi}\frac{\omega_{\rm eff}^2}{\Gamma_{\rm eff}-i\omega}\ , \tag{1}$$

where

$$\Gamma_{\rm eff}=\frac{\Gamma(\omega)}{1+\lambda(\omega)}\ , \tag{2}$$

and

$$\omega_{\rm eff}^2=\frac{\omega_p^2}{1+\lambda(\omega)}\ . \tag{3}$$

One can determine $\lambda(\omega)$ and $\Gamma(\omega)$ from the Kramers-Kronig-derived dielectric functions using the following equations:

$$\Gamma(\omega)=\frac{\omega_p^2}{\omega}\frac{\epsilon_2}{\epsilon_1^2+\epsilon_2^2}\ , \tag{4}$$

$$\lambda(\omega)=\frac{\omega_p^2}{\omega^2}\frac{\epsilon_1}{\epsilon_1^2+\epsilon_2^2}-1\ . \tag{5}$$

The generalized Drude formalism applies only to the itinerant carriers in the system and any interband or phonon contributions to $\epsilon_1(\omega)$ and $\epsilon_2(\omega)$ must be subtracted before calculating the frequency-dependent mass enhancements $\lambda(\omega)$ and scattering rate $\Gamma(\omega)$. To obtain $\lambda(\omega)$ and $\Gamma(\omega)$ using Eqs. (4) and (5), we first calculate $\epsilon_1(\omega)$ and $\epsilon_2(\omega)$ using Kramers-Kronig analysis, then subtract the high-frequency and phonon contributions to the dielectric function using the parameters listed in Table II. One also needs to know the unrenormalized carrier density ($\propto\omega_p^2$). In the absence of Hall-effect data, one can estimate that the carrier density is equal to $(1.6\times10^{22}\ {\rm cm}^{-3})(1-3x)$, which assumes *n*-type carriers in a single conduction band consistent with the Hall measurements of Tokura *et al.* for $La_xSr_{1-x}TiO_3$.[5] Using the chemical data of Table I, the carrier densities work out to be 1.3×10^{22} cm^{-3} and 1.0×10^{22} cm^{-3} for samples *C* and *D*, respectively. The frequency-dependent mass enhancements and scattering rates for samples *C* and *D* appear in Fig. 8. At 300 cm^{-1}, $\lambda(\omega)$ is significantly larger for sample *C*, with a larger number of electrons as-

sociated with the Ti $3d$ band, than sample D. Fujishima *et al.*[10] obtained a similar result at 0.1 eV (800 cm^{-1}) for $La_xSr_{1-x}TiO_3$. However, below about 100 cm^{-1}, which is below the lower limit of the data of Fujishima *et al.*, we observe that $\lambda(\omega)$ becomes negative for sample C.

There are two problems with this analysis. To begin, the large scattering rate implies a mean free path less than a lattice constant for sample C. Second, one has to explain the negative mass enhancement at low frequencies. Negative mass enhancements in the generalized Drude formalism are difficult to interpret but are associated with a low frequency $\sigma(\omega)$ that *increases* monotonically with frequency. However, the optical properties and transport properties should be consistent in the following sense: Examination of various theoretical models show that $\lambda(\omega)$ has the same sign as $d\Gamma(\omega)/d\omega$ and, physically, $d\Gamma(\omega)/d\omega$ should have the same sign as $d\rho/dT$ where $\rho(T)$ is the dc resistivity. This consistency between the optical and transport properties can be seen experimentally in URu_2Si_2, where both the temperature coefficient of the dc resistivity and low-frequency $\lambda(\omega)$ are positive below 70 K and negative above 70 K.[34,36] One can contrast the URu_2Si_2 data with $La_{1-x}TiO_3$ sample C where the low-frequency $\lambda(\omega)$ is negative, but the dc resistivity increases with temperature as shown in Fig. 1.

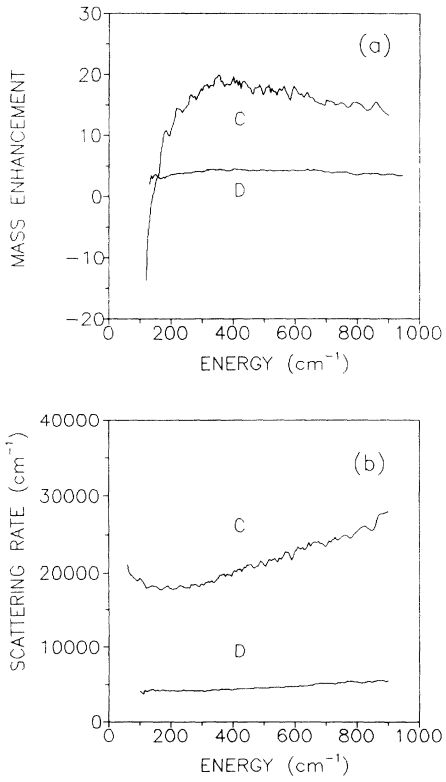

FIG. 8. Frequency-dependent (a) mass-enhancement factors $\lambda(\omega)$ and (b) scattering rates $\Gamma(\omega)$ for samples C and D after subtracting out the phonon, ϵ_∞, and charge-transfer oscillator contributions to the dielectric functions.

Thus, one could argue that in $La_{1-x}TiO_3$ any filling-dependent mass enhancement is obscured in the optical data by the presence of the midinfrared band. For sample C, one should subtract a midinfrared component from ϵ_1 and ϵ_2 in addition to the phonon and high-frequency contributions before calculating $\lambda(\omega)$ and $\Gamma(\omega)$. In practice, this is impossible because the actual shape of the midinfrared component is not known. Cao *et al.* have analyzed the non-Drude optical properties of the heavy-fermion material UNi_2Si_2 by first fitting the reflectance to a dielectric function consisting of a Drude plus midinfrared oscillators. After subtracting the midinfrared components, they analyzed the remainder for $\lambda(\omega)$ and $\Gamma(\omega)$ and found mass enhancement below the coherence temperature.[37] If one attempts this procedure for $La_{1-x}TiO_3$, one finds that the remainder is only the Drude component with a frequency-independent scattering rate. Thus, it appears that the frequency-dependent scattering-rate analysis is not appropriate for this system.

V. CONCLUSIONS

One finds that the low-frequency optical conductivity of samples on the metallic side of the doping-induced phase transition from Mott-insulator ($LaTiO_3$) to highly correlated metal ($La_{1-x}TiO_3$) increases with frequency in a manner similar to other barely metallic systems. In the $La_{1-x}TiO_3$ system, there are two low-frequency contributions to the optical conductivity: the response of the itinerant carriers and a midinfrared band. It would be useful to study the low-frequency reflectance of metallic samples of $Y_xCa_{1-x}TiO_3$ or $Nd_{1-x}TiO_3$ where it may be possible to remove the midinfrared contribution before calculating the frequency-dependent scattering rate and mass enhancement. The data indicate that the midinfrared band persists in highly doped samples in agreement with theoretical studies, which show the feature in the optical conductivity associated with the upper Hubbard band exists even when only half the sites are filled. Temperature-dependent studies of highly doped n-type $SrTiO_3$ are being made in order to see whether the temperature dependence of the midinfrared band is similar to the temperature dependence of the band in $LaTiO_3$. Finally, it has been established that $LaTiO_3$ is susceptible to La vacancies, which can induce the insulator-metal transition. X-ray studies on $La_{1-x}TiO_3$ and $Nd_{1-x}TiO_3$ are in progress, which should verify the rare-earth vacancy model for other rare-earth titanites.

ACKNOWLEDGMENTS

We wish to thank Wen He Gong, Frank Gibbs, and Alice Pidruczny for the x-ray, thermogravimetric, neutron activation analysis, respectively. We acknowledge discussions with D. A. Bonn and Walter Stephan. This work was supported at McMaster by the Natural Science and Engineering Research Council of Canada including infrastructure support for the Institute for Materials Research.

[1]F. Lichtenberg, T. Williams, A. Reller, D. Widmer, and J. G. Bednorz, Z. Phys. B **84**, 369 (1991).
[2]D. A. Crandles, T. Timusk, J. D. Garrett, and J. E. Greedan, Physica C **201**, 407 (1992).
[3]J. E. Greedan, J. Less Common Metals **111**, 335 (1985).
[4]Y. Okada, T. Arima, Y. Tokura, C. Murayama, and N. Môri, Phys. Rev. B **48**, 9677 (1993).
[5]Y. Tokura, Y. Taguchi, Y. Okada, Y. Fujishima, T. Arima, K. Kumagai, and Y. Iye, Phys. Rev. Lett. **70**, 2126 (1992).
[6]K. Kumagai, T. Suzuki, Y. Taguchi, Y. Okada, Y. Fujishima, and Y. Tokura, Phys. Rev. B **48**, 7636 (1993).
[7]J. E. Sunstrom IV, S. M. Kauzlarich, and P. Klavins, Chem. Mater. **4**, 346 (1992).
[8]Y. Maeno, S. Awaji, H. Matsumoto, and T. Fujita, Physica B **165/166**, 1185 (1990).
[9]A. Fujimori, I. Hase, M. Nakamura, H. Namatame, Y. Fujishima, Y. Tokura, M. Abbate, F. M. F. de Groot, M. T. Czyzyk, J. C. Fugle, O. Strebel, F. Lopez, M. Domke, and G. Kaindl, Phys. Rev. B **46**, 9841 (1992).
[10]Y. Fujishima, Y. Tokura, T. Arima, and S. Uchida, Physica C **185-189**, 1001 (1991); Phys. Rev. B **46**, 11 167 (1992).
[11]J. Zaanen, G. A. Sawatsky, and J. W. Allen, Phys. Rev. Lett. **55**, 418 (1985).
[12]S. L. Cooper, G. A. Thomas, J. Orenstein, D. H. Rapkine, A. J. Millis, S-W. Cheong, and A. S. Cooper, Phys. Rev. B **41**, 11 605 (1990).
[13]S. Uchida, T. Ido, H. Takagi, T. Arima, Y. Tokura, and S. Tajima, Phys. Rev. B **43**, 7942 (1991).
[14]M. Reedyk, T. Timusk, J. S. Xue, and J. E. Greedan, Phys. Rev. B **45**, 7406 (1992).
[15]T. Ido, K. Magoshi, H. Eisaki, and S. Uchida, Phys. Rev. B **44**, 12 094 (1991).
[16]Y. Taguchi, Y. Tokura, T. Arima, and F. Inaba, Phys. Rev. B **48**, 511 (1993).
[17]M. Kasuya, Y. Tokura, T. Arima, H. Eisaki, and S. Uchida, Phys. Rev. B **47**, 6197 (1993).
[18]D. A. Maclean, H-N. Ng, and J. E. Greedan, J. Solid State Chem. **30**, 35 (1979).
[19]J. P. Goral and J. E. Greedan, J. Magn. Magn. Mater. **37**, 315 (1983).
[20]M. Abe and K. Uchino, Mater. Res. Bull. **9**, 147 (1974).
[21]C. C. Homes, M. Reedyk, D. A. Crandles, and T. Timusk, Appl. Opt. **32**, 2976 (1993).
[22]M. A. Cardona, Phys. Rev. **140**, A651 (1965).
[23]H. Eskes, M. B. J. Meinders, and G. A. Sawatsky, Phys. Rev. Lett. **67**, 1035 (1991).
[24]A. S. Barker, Jr. and J. P. Remeika, Solid State Commun. **8**, 1521 (1970).
[25]C. C. Homes, T. Timusk, X. Wu, Z. Altounian, A. Sahnoune, and J. O. Ström-Olsen, Phys. Rev. Lett. **67**, 2694 (1991).
[26]H. F. Jang, G. Cripps, and T. Timusk, Phys. Rev. B **41**, 5152 (1990).
[27]J. B. Torrance, P. Lacorre, Chinnarong Asavaroengchai, and R. M. Metzger, J. Solid State Chem. **90**, 168 (1991).
[28]A. Fujimori, I. Hase, H. Namatame, Y. Fujishima, Y. Tokura, H. Eisaki, S. Uchida, K. Takegahara, and F. M. F. de Groot, Phys. Rev. Lett. **69**, 1796 (1992).
[29]W. Stephan and P. Horsch, Phys. Rev. B **42**, 8736 (1990).
[30]A. S. Barker, Jr., *Proceedings of the International Colloquium on the Optical Properties and Electronic Structure of Metals and Alloys, Paris, 1965* (North-Holland, Amsterdam, 1966).
[31]H. G. Reik, Z. Phys. **203**, 346 (1967).
[32]P. Calvani, M. Capizzi, F. Donato, S. Lupi, P. Maselli, and D. Peschiaroli, Phys. Rev. B **47**, 8917 (1993).
[33]J. W. Allen and J. C. Mikkelsen, Phys. Rev. B **15**, 2952 (1977).
[34]D. A. Bonn, J. D. Garrett, and T. Timusk, Phys. Rev. Lett. **61**, 1305 (1988).
[35]J. W. Allen and J. C. Mikkelsen, Phys. Rev. B **15**, 2952 (1977).
[36]T. T. Palstra, A. A. Menovsky, and J. A. Mydosh, Phys. Rev. B **33**, 6527 (1986).
[37]N. Cao, J. D. Garrett, and T. Timusk, Physica B **191**, 263 (1993).